J|A|C|S
ARTICLES
Published on Web 01/21/2004

Radical Clock Substrates, Their C−H Hydroxylation Mechanism by Cytochrome P450, and Other Reactivity Patterns: What Does Theory Reveal about the Clocks' Behavior?

Devesh Kumar, Samuël P. de Visser, Pankaz K. Sharma, Shimrit Cohen, and Sason Shaik*

Contribution from the Department of Organic Chemistry and the Lise-Meitner-Minerva Center for Computational Quantum Chemistry, The Hebrew University of Jerusalem, 91904 Jerusalem, Israel

Received November 5, 2003; E-mail: sason@yfaat.ch.huji.ac.il

Abstract: There is an ongoing and tantalizing controversy regarding the mechanism of a key process in nature, C−H hydroxylation, by the enzyme cytochrome P450 (Auclaire, K.; Hu, Z.; Little, D. M.; Ortiz de Montellano, P. R.; Groves, J. T. *J. Am. Chem. Soc.* **2002**, *124*, 6020−6027. Newcomb, M.; Aebisher, D.; Shen, R.; Esala, R.; Chandrasena, P.; Hollenberg, P. F.; Coon, M. J. *J. Am. Chem. Soc.* **2003**, *125*, 6064−6065). To definitely resolve this controversy, theory must first address *the actual systems that have been used by experiment*, and that generated the controversy. This is done in the present paper, which constitutes the first extensive theoretical study *of such two experimental systems*, *trans*-2-phenylmethyl-cyclopropane (**1**) and *trans*-2-phenyl-*iso*-propylcyclopropane (**4**). The theoretical study of these substrates reveals that the only low energy pathway for C−H hydroxylation is *the two-state rebound mechanism* described originally for methane hydroxylation (Ogliaro, F.; Harris, N.; Cohen, S.; Filatov, M.; de Visser, S. P.; Shaik, S. *J. Am. Chem. Soc.* **2000**, *122*, 8977−8989). The paper shows that the scenario of a two-state rebound mechanism accommodates much of the experimental data. The computational results provide a good match to experimental results concerning the very different extents of rearrangement for **1** (20−30%) vs **4** (virtually none), lead to *product isotope effect* for the reaction of **1**, in the direction of the experimental result, and predict as well the observed metabolic switching from methyl to phenyl hydroxylation, which occurs upon deuteration of the methyl group. Furthermore, the study reveals that an intimate ion pair species involving an alkyl carbocation derived from **4** gives no rearranged products, again in accord with experiment. *This coherent match between theory and experiment cannot be merely accidental; it comes close to being a proof that the actual mechanism of C−H hydroxylation involves the two-state reactivity revealed by theory.* Analysis of the rearrangement modes of the carbocations derived from **1** and **4** excludes the participation of free carbocations during the hydroxylation of these substrates. Finally, the mechanistic significance of product isotope effect (different isotope effects for the rearranged and unrearranged alcohol products) is analyzed. It is shown to be a sensitive probe of two-state reactivity; the size of the intrinsic product isotope effect and its direction reveal the structural differences of the hydrogen abstraction transition states in the low-spin vs high-spin reaction manifolds.

1. Introduction

C−H hydroxylation is one of the Holy Grails in Chemistry. In Nature, this process is achieved by the enzyme cytochrome P450, which is one of the most potent monooxygenating enzymes in aerobic organisms.[1] The primary active species of the enzyme is the high valent iron−oxo species called Compound I (Cpd I), Scheme 1. Indeed, artificial Cpd I species were made early on[2,3] and shown to perform C−H hydroxylation[4] and other monooxygenation processes typical to P450. In 1976, Groves and McClusky[5] suggested a reaction mechanism for C−H hydroxylation by Cpd I, which accommodated the known facts; this is the "rebound mechanism" shown in Scheme 1. The first step in this mechanism involves hydrogen abstraction from the alkane (Alk-H) by Cpd I. Subsequently, the alkyl radical can either instantly rebound to form an alcohol complex, where the alcohol is unrearranged (*U*), keeping the original stereochemical integrity of the alkane, or first undergo skeletal rearrangement and then rebound to give a rearranged (*R)* alcohol product. The rebound mechanism accounts for partial loss of

(1) *Cytochrome P450: Structure, Mechanisms and Biochemistry*, 2nd ed.; Ortiz de Montellano, P. R., Ed.; Plenum Press: New York, 1995.
(2) (a) Groves, Y.-Z.; Han, J. T. In *Cytochrome P450: Structure, Mechanism and Biochemistry*, 2nd ed.; Ortiz de Montellano, P. R., Ed.; Plenum Press: New York, 1995; pp 3−48. (b) Groves, J. T. *Proc. Natl. Acad. Sci. U.S.A.* **2003**, *100*, 3569−3574.
(3) Groves, J. T. *J. Chem. Educ.* **1985**, *62*, 928−931.
(4) Groves, J. T.; McClusky, G. A.; White, R. E.; Coon, M. J. *Biochem. Biophys. Res. Commun.* **1978**, *81*, 154−160.
(5) Groves, J. T.; McClusky, G. A. *J. Am. Chem. Soc.* **1976**, *98*, 859−861.

Scheme 1. Cpd I, the Rebound Mechanism (Refs 2 and 6) and the Apparent Radical Lifetime (τ_{Alk})

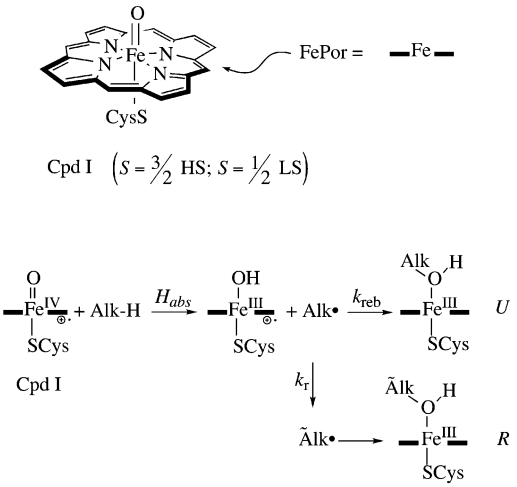

$$\tau_{Alk} = \frac{1}{k_r}\left[\frac{R}{U}\right]$$

stereochemistry and geometrical rearrangement data,[6] as well as for the large intrinsic kinetic isotope effect (KIE) observed[4−14] when the hydrogen in transit is replaced by deuterium. The large extent of stereoselectivity (>90%)[6b] and the occasional stereospecificity[10,12] suggested that the radicals are rather short-lived.

The first experiment to determine the lifetime of the radical was carried out by Ortiz de Montellano and Stearns,[13] using bicyclo[2.1.0]pentane. The measured ratio of unrearranged to rearranged products [*U*/*R*] and the free radical rearrangement rate constant, k_r (Scheme 1), enabled them to measure the lifetime of the radical as $\tau = 50$ ps. Other studies of radical clocks followed and generated a variety of lifetime data, which indicated that the radicals formed during the reactions are short-lived and have selectively restricted motions.[6b]

The support for the rebound mechanism looked solid until Newcomb et al.[15−18] began their investigation of ultrafast radical clocks and carbocationic clocks. Thus, Newcomb has shown that the quantity [*U*/*R*] for a series of radical clocks does not correlate with the known lifetimes of the putative free radical

Scheme 2. Two-Oxidant Mechanism of P450 (Ref 15) and Probe Substrate That Can Distinguish between Radical- and Cation-Type Rearrangements by Opening as Indicated by the Wiggly Arrows

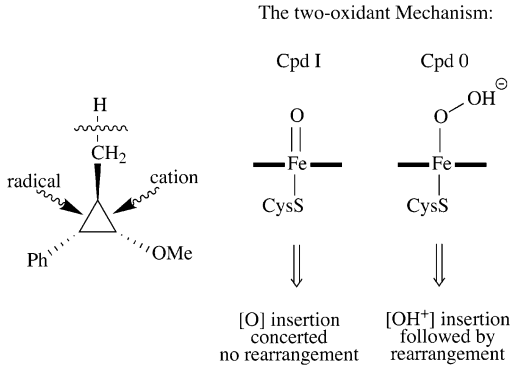

clocks.[15] Some rearrangement patterns of clocks such as the one depicted in Scheme 2 were shown to correspond to carbocationic species.[16,18,19] In other substrates, the rearrangement patterns between radicals and cations are considered to be the same so that they cannot be distinguished.[15] Thus, wherever possible, subtraction of these carbocationic rearrangements from the overall product mixture resulted in lifetimes as short as even 70 fs,[16,18] too short to qualify as lifetimes of real intermediate species. These unrealistically short lifetimes and the rearranged products derived from carbocations have led Newcomb and co-workers[15] to suggest that radical intermediates are not present during the reaction and that alkane hydroxylation proceeds by two competing mechanisms nascent from two oxidant species of the enzyme, Cpd I and its precursor ferric hydroperoxide species, so-called Cpd 0 (Scheme 2). As shown in Scheme 2, the "two-oxidant mechanism" does not involve any radical intermediates; Cpd I is suggested to perform an effectively concerted [O]-insertion into the C−H bond, while Cpd 0 inserts a hydroxonium ion (OH^+) into the C−H bond. This latter process generates a protonated alcohol, which subsequently rearranges in a manner typical to a carbocation. Thus, Newcomb et al.[15] reject the rebound mechanism and its radical intermediate and suggest to replace it by the two-oxidant (Cpd I and Cpd 0) mechanism.

While there exists recent indirect evidence for the reactivity of Cpd 0, however sluggish, this evidence is restricted to double bond epoxidation,[20] and it occurs only in the supression of Cpd I in the system. Furthermore, the cryogenic EPR and ENDOR follow-up,[21] during camphor hydroxylation, support hydroxylation by Cpd I but not by Cpd 0. Theory lends support to this conclusion by showing that Cpd 0 is a sluggish oxidant toward double bond epoxidation[22,23] and sulfoxidation,[24] let alone hydroxylation. Thus, the two-oxidant mechanism is not reconcilable with what is known on the reactivity of Cpd 0, from experiment or theory. And, at this stage of knowledge, the balance is in favor of C−H hydroxylation occurring only by

(6) (a) Ortiz de Montellano, P. R.; De Voss, J. J. *Nat. Prod. Rep.* **2002**, *19*, 1−18. (b) Auclaire, K.; Hu, Z.; Little, D. M.; Ortiz de Montellano, P. R.; Groves, J. T. *J. Am. Chem. Soc.* **2002**, *124*, 6020−6027.
(7) Sorokin, A.; Robert, A.; Meunier, B. *J. Am. Chem. Soc.* **1993**, *115*, 7293−7299.
(8) Gelb, M. H.; Heimbrook, D. C.; Mälkönen, P.; Sligar, S. G. *Biochemistry* **1982**, *21*, 370−377.
(9) Sono, M.; Roach, M. P.; Coulter, E. D.; Dawson, J. H. *Chem. Rev.* **1996**, *96*, 2841−2888.
(10) Woggon, W.-D. *Top. Curr. Chem.* **1996**, *184*, 39−95.
(11) Meunier, B.; Bernadou, J. *Top. Catal.* **2002**, *21*, 47−55.
(12) Fretz, H.; Woggon, W.-D.; Voges, R. *Helv. Chim. Acta* **1989**, *72*, 391−400.
(13) Ortiz de Montellano, P. R.; Stearns, R. A. *J. Am. Chem. Soc.* **1987**, *109*, 3415−3420.
(14) (a) Audergon, C.; Iyer, K. R.; Jones, J. P.; Darbyshire, J. F.; Trager, W. T. *J. Am. Chem. Soc.* **1999**, *121*, 41−47. (b) Manchester, J. I.; Dinnocenzo, J. P.; Higgins, L. A.; Jones, J. P. *J. Am. Chem. Soc.* **1997**, *119*, 5069−5070.
(15) Newcomb, M.; Toy, P. H. *Acc. Chem. Res.* **2000**, *33*, 449−455.
(16) Newcomb, M.; Shen, R.; Choi, S.-Y.; Toy, P. H.; Hollenberg, P. F.; Vaz, A. D. N.; Coon, M. J. *J. Am. Chem. Soc.* **2000**, *122*, 2677−2686.
(17) Toy, P. H.; Newcomb, M.; Hollenberg, P. F. *J. Am. Chem. Soc.* **1998**, *120*, 7719−7729.
(18) Newcomb, M.; Le Tadic-Biadatti, M.-H.; Chestney, D. L.; Roberts, E. S.; Hollenberg, P. F. *J. Am. Chem. Soc.* **1995**, *117*, 12085−12091.
(19) Newcomb, M.; Shen, R.; Lu, Y.; Coon, M. J.; Hollenberg, P. F.; Kopp, D. A.; Lippard, S. J. *J. Am. Chem. Soc.* **2002**, *124*, 6879−6886.
(20) Jin, S.; Makris, T. M.; Bryson, T. A.; Sligar, S. G.; Dawson, J. H. *J. Am. Chem. Soc.* **2003**, *125*, 3406−3407.
(21) Davydov, R.; Makris, T. M.; Kofman, V.; Werst, D. E.; Sligar, S. G.; Hoffman, B. M. *J. Am. Chem. Soc.* **2001**, *123*, 1403−1415.
(22) Ogliaro, F.; de Visser, S. P.; Cohen, S.; Sharma, P. K.; Shaik, S. *J. Am. Chem. Soc.* **2002**, *124*, 2806−2817.
(23) Kamachi, T.; Shiota, Y.; Ohta, T.; Yoshizawa, K. *Bull. Chem. Soc. Jpn.* **2003**, *76*, 721−732.
(24) Sharma, P. K.; de Visser, S. P.; Shaik, S. *J. Am. Chem. Soc.* **2003**, *125*, 8698−8699.

reaction with Cpd I. Despite this assessment of the two-oxidant hypothesis, Newcomb has raised an important issue, namely that *the experimental results strongly imply that the products of hydroxylation behave as though they originate from two different sources*. But what are these sources?

Theory[25−29] offered already a reasonable resolution of the main elements in this mechanistic controversy, by suggesting[25−27] the two-state reactivity (TSR) mechanism, which is nascent from the two degenerate states of Cpd I. Thus, Cpd I has closely lying doublet and quartet spin states (Scheme 1), which are referred to as the low-spin (LS) and high-spin (HS) states. These states lead, in turn, to corresponding rebound mechanisms. The HS and LS energy profiles were found to be close in energy, all the way to the PorFeOH/Alk• cluster, and subsequently they bifurcated. In the LS manifold, once the radical snaps out of the weak C- - -HO interaction with the iron hydroxo species, the ensuing LS rebound phase itself is a barrierless process.[25−27] By contrast, the HS process has a significant barrier to rebound, with a real transition state. As such, the radical intermediate will have a sufficiently long lifetime on the HS manifold, and an ultrashort one, or altogether zero lifetime, on the LS manifold. Extending this picture to a radical lifetime determination (Scheme 1) means that the amount of rearranged products *R* originates mainly in the HS state, while the unrearranged product *U* is contributed by both HS and LS states or mostly by the LS state. Thus, the apparent radical lifetime, which is quantitated from the ratio [*U*/*R*], is not a genuine lifetime, since it also reflects the relative yields of the HS and LS processes. As a rule, since the LS surface in C−H hydroxylation lies below the HS, the quantity [*U*/*R*] will yield apparent lifetimes that are shorter than the real ones. Thus, TSR[25,27] reveals a two-state rebound mechanism, which on one hand accommodates the KIE evidence that indicates a hydrogen abstraction-like transition state in the bond activation and on the other hand demonstrates how a two-state rebound step can lead to seemingly controversial lifetimes if one assumes that the [*U*/*R*] quantity is a result of a single radical intermediate that is rapidly partitioned between instant rebound and rearrangement followed by rebound, as in Scheme 1. *The question is whether the TSR scenario can really account for the various facets of clock behavior?*

In a recent paper, Newcomb et al.[30] presented kinetic isotopic studies, which indicated that the rearranged, *R*, and unrearranged, *U*, products of the clock substrate, *trans*-2-phenyl-methyl cyclopropane, **1**, respond differently to isotopic substitution of the scissile C−H bonds. Thus, as shown in Scheme 3, the kinetic isotope effect of *U*, **2**, is larger than that of *R*, **3**, such that there exists product isotope effect (PIE), which is greater than unity, i.e., PIE[*U*,**2**/*R*,**3**] > 1. A PIE different from unity rules out the possibility that the two products arise from a common intermediate, i.e., from a single pathway, and would therefore support a mechanistic scenario with two different "processes".

Scheme 3. Rearranged (*R*) and Unrearranged (*U*) Products of the Probe Substrate **1**, the Observed Product Isotope Effect (*PIE*), and Substrate **4** with Its Sole Observed Product **5**

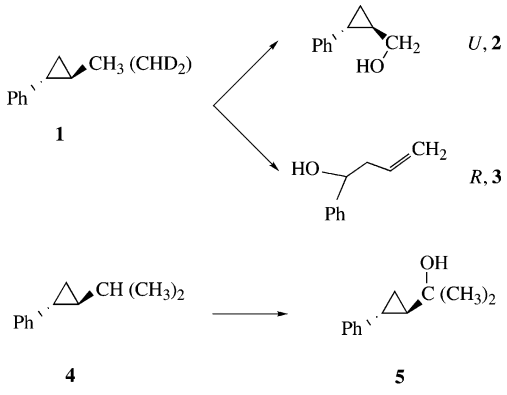

$$PIE[U,\mathbf{2}/R,\mathbf{3}] = \frac{KIE(\mathbf{2})}{KIE(\mathbf{3})} > 1$$

A priori, PIE ≠ 1 may indicate either TSR or a two-oxidant mechanism (Scheme 2). The existence of PIE ≠ 1 was anticipated by Ogliaro et al.,[31] in terms of the two-state scenario. TSR predicts that in principle, since *U* and *R* originate from two different hydrogen abstraction transition states, the observed PIE can be different from unity. However, as pointed out by Newcomb et al.,[30] using the TSR results for methane hydroxylation[31] or allylic hydroxylation[32] would lead to PIE < 1, precisely in the opposite direction to the experimentally measured quantity, i.e., *PIE*[*U*,**2**/*R*,**3**] > 1. For this reason, Newcomb et al. concluded that their results rule out TSR and support the two-oxidant mechanism. But, as argued above, the two-oxidant mechanism for C−H hydroxylation is not reconcilable with what is known from experiment and theory. Therefore, the central question is whether the TSR model can really be ruled out or admitted on the basis of the abstract PIE values of these model substrates? The resolution of this important mechanistic puzzle requires not only a proof of principle but also a direct calculation of C−H hydroxylation of a Newcomb probe and a theoretical determination of the PIE[*U*,**2**/*R*,**3**] quantity. As demonstrated in a preliminary communication,[33] the calculation of C−H hydroxylation of **1**, exhibits TSR and the computed PIE[*U*,**2**/*R*,**3**] quantity matches experiment quite well. As the title of the present paper implies, there remains, however, a host of mechanistic puzzles and issues that are posed by the Newcomb probes and which requires answers in order to resolve the controversy as a whole.

The present paper uses density functional theoretical (DFT) calculations to elucidate the hydroxylation mechanisms of two Newcomb probe substrates, **1** and **4** (Scheme 3), and addresses the following issues. First, we shall try to establish the mechanistic significance of PIE[*U*/*R*] as an indicator of the geometric differences in the HS vs LS transition states for hydrogen abstraction and the dependence of this quantity on the nature of the substrate and its overall reactivity. Then we shall attempt to understand why **1** leads to substantial rear-

(25) Ogliaro, F.; Harris, N.; Cohen, S.; Filatov, M.; de Visser, S. P.; Shaik, S. *J. Am. Chem. Soc.* **2000**, *122*, 8977−8989.
(26) de Visser, S. P.; Ogliaro, F.; Harris, N.; Shaik, S. *J. Am. Chem. Soc*. **2001**, *123*, 3037−3047.
(27) Shaik, S.; de Visser, S. P.; Ogliaro, F.; Schwarz, H.; Schröder, D. *Curr. Opin. Chem. Biol*. **2002**, *6*, 556−567
(28) Yoshizawa, K.; Kamachi, T.; Shiota, Y. *J. Am. Chem. Soc.* **2001**, *123*, 9806−9816.
(29) Kamachi, T.; Yoshizawa, K. *J. Am. Chem. Soc.* **2003**, *125*, 4652−4661.
(30) Newcomb, M.; Aebisher, D.; Shen, R.; Esala, R.; Chandrasena, P.; Hollenberg, P. F.; Coon, M. J. *J. Am. Chem. Soc.* **2003**, *125*, 6064−6065.
(31) Ogliaro, F.; Filatov, M.; Shaik, S. *Eur. J. Inorg. Chem*. **2000**, 2455−2458.
(32) de Visser, S. P.; Ogliaro, F.; Sharma, P. K.; Shaik, S. *J. Am. Chem. Soc.* **2002**, *124*, 11809−11826.
(33) Kumar, D.; de Visser, S. P.; Shaik, S. *J. Am. Chem. Soc.* **2003**, *125*, 13024−13025.

rangement, while **4** gives virtually no rearranged product.[15] Another issue is the metabolic switching, from C−H hydroxylation to phenyl hydroxylation that accompanies the complete deuteration of the methyl group in **1**.[15] Combining our recent calculations of benzene hydroxylation[34] with the present ones will enable us to assess this delicate balance of the regioselectivity switching and its mechanistic significance. An open ended issue concerns the relationship between the rearrangement barriers of the complexed radicals, PorFeOH/Alk•, vis-à-vis the rearrangement of the free radicals: Does complexation change the barriers for rearrangements drastically to the extent that the lifetimes determined by use of the free radical clock data are incorrect? Finally, by comparing the PorFeOH/Alk intermediates for clock substrates **1** vs **4**, we shall address the question of how and if carbocations do incur during the reaction? In short, we would like to answer the question: *what does the clock actually tell us about P450 hydroxylation*?

2. Methods

All methods used here were similar to those in our previous studies and are summarized. The systems were modeled using the unrestricted hybrid density functional UB3LYP[35] combined with an LACVP basis set[36] on iron and 6-31G basis sets on the remaining atoms (hence UB3LYP/LACVP). Single-point calculations were done with a triple-ζ basis set, which includes polarization and diffuse functions on all non-hydrogen atoms (hence UB3LYP/LACV3P^{+}*).[37] All calculations were performed using the Jaguar 4.1[37] and GAUSSIAN 98[38] program packages. The study generated a large amount of data (spin densities, charge distributions, detailed geometries, potential energy scans, etc.), which are useful but cannot be included in the paper for space economy. These are relegated to the Supporting Information.

Cpd I (Scheme 1) was modeled as an iron−oxo−porphine complex, where the proximal thiolate ligand was truncated to SH$^-$.[25,26] The effect of hydrogen bonding to the sulfur ligand was mimicked by adding two ammonia molecules to the system which pointed toward the sulfur of the proximal ligand at fixed distances of $r_{S-HN} = 2.660$ Å.[39] The effect of polarization by the electric field was studied using the efficient continuum solvent model implemented in Jaguar 4.1 with a dielectric constant of $\epsilon = 5.7$ (and probe radius 2.72 Å). A recent QM/MM study[40] in collaboration with the Mülheim group shows that the SH$^-$ ligand along with these simple mimicks of the environmental effects represents the state of Cpd I in the protein pocket quite well.[41] This conclusion is reinforced by recent QM/MM studies of camphor hydroxylation.[42]

Full optimization of all structures was carried out with the fast Jaguar 4.1 program package. Initially, geometry scans were generated in which one variable served as the "reaction coordinate", while all the remaining degrees of freedom were fully optimized. The scans gave information about the potential energy surface between the transition states and the local minima and were used to connect the transition states with the local minima and vice versa. All these scans are included in the Supporting Information as Figures S.1, S.4−S.6, S.9−S.11, S.14, S.18, S.19, and S.22. Subsequently, all transition states and intermediates were located by free optimization and characterized by frequency calculations, using GAUSSIAN 98 that computes analytical frequencies. All transition states mentioned hereafter had one imaginary frequency each. It is important to note that the rebound transition states are more easily located if one starts from a conformation where the alkyl radical attacks in a 90° angle or so to the OH bond of the iron−hydroxo species (see the $\mathbf{I}_U$ species in Scheme 4). Otherwise, many difficulties are encountered during the transition state search.

Scheme 4 Schematic Representation of the Species Located in the Study, for Probe **1**, and Their Designations[a]

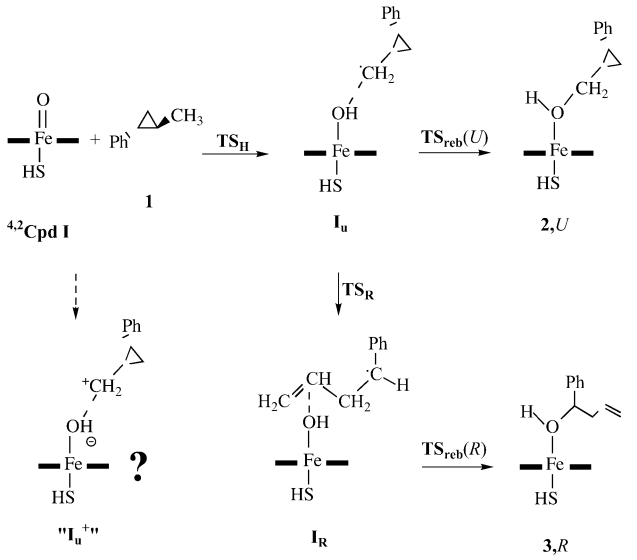

[a] Part of these species are located also for probe **4**, and have the same labels.

Single-point energy calculations on the optimized structures were employed to obtain the effects of NH- - -S hydrogen bonding and solvation by a dielectric medium. In our experience, the solvent calculations with Jaguar 4.1 occasionally give different solvation energies of two separate molecules and their supermolecule at a large intermolecular distance (of 10 Å). We therefore refrain from calculating absolute barriers relative to the separate reactants with $\epsilon = 5.7$ and prefer to compare relative transition state energies.

Location of carbocationic states, PorFeOH($^-$)/Alk$^+$, is done by swapping an electron from the alkyl radical to the singly occupied π*-(d_{xz}) orbital of the iron−hydroxo species, while reoptimizing the orbitals by the SCF procedure (using the option vshift = 10; see Table S.20 in the Supporting Information). When this is done at the geometries of the $^{2,4}\mathbf{I}_u$ species, the resulting cation species state is a vertical state, while subsequently allowing for geometry optimization generates the optimized PorFeOH($^-$)/Alk$^+$ states.

The kinetic isotope effect (KIE) of the hydroxylation reaction was determined using the GAUSSIAN data based on three models.[43] The

(34) de Visser, S. P.; Shaik, S. *J. Am. Chem. Soc.* **2003**, *125*, 7413−7424.
(35) (a) Becke, A. D. *J. Chem. Phys.* **1992**, *96*, 2155. (b) Becke, A. D. *J. Chem. Phys.* **1992**, *97*, 9173. (c) Becke, A. D. *J. Chem. Phys.* **1993**, *98*, 5648. (d) Lee, C.; Yang, W.; Parr, R. G. *Phys. Rev. B* **1988**, *37*, 785.
(36) (a) Hay, J. P.; Wadt, W. R. *J. Chem. Phys.* **1985**, *82*, 99. (b) Friesner, R. A.; Murphy, R. B.; Beachy, M. D.; Ringlanda, M. N.; Pollard, W. T.; Dunietz, B. D.; Cao, Y. X. *J. Phys. Chem. A* **1999**, *103*, 1913.
(37) *Jaguar 4.1*; Schrödinger, Inc.: Portland, OR, 2000.
(38) Frisch, M. J.; Trucks, G. W.; Schlegel, H. B.; Scuseria, G. E.; Robb, M. A.; Cheeseman, J. R.; Zakrzewski, V. G.; Montgomery, J. A., Jr.; Stratmann, R. E.; Burant, J. C.; Dapprich, S.; Millam, J. M.; Daniels, A. D.; Kudin, K. N.; Strain, M. C.; Farkas, O.; Tomasi, J.; Barone, V.; Cossi, M.; Cammi, R.; Mennucci, B.; Pomelli, C.; Adamo, C.; Clifford, S.; Ochterski, J.; Petersson, G. A.; Ayala, P. Y.; Cui, Q.; Morokuma, K.; Malick, D. K.; Rabuck, A. D.; Raghavachari, K.; Foresman, J. B.; Cioslowski, J.; Ortiz, J. V.; Stefanov, B. B.; Liu, G.; Liashenko, A.; Piskorz, P.; Komaromi, I.; Gomperts, R.; Martin, R. L.; Fox, D. J.; Keith, T.; Al-Laham, M. A.; Peng, C. Y.; Nanayakkara, A.; Gonzalez, C.; Challacombe, M.; Gill, P. M. W.; Johnson, B. G.; Chen, W.; Wong, M. W.; Andres, J. L.; Head-Gordon, M.; Replogle, E. S.; Pople, J. A. *Gaussian 98*; Gaussian, Inc.: Pittsburgh, PA, 1998.
(39) (a) Ogliaro, F.; Cohen, S.; de Visser, S. P.; Shaik, S. *J. Am. Chem. Soc.* **2000**, *122*, 12892−12893. (b) Ogliaro, F.; de Visser, S. P.; Cohen, S.; Kaneti, J.; Shaik, S. *ChemBioChem* **2001**, *2*, 848−851.
(40) Schöneboom, J. C.; Reuter, N.; Lin, H.; Thiel, W.; Cohen, S.; Ogliaro, F.; Shaik, S. *J. Am. Chem. Soc.* **2002**, *124*, 8142−8151.
(41) For a recent review on Cpd I, see: Harris, D. L. *Curr. Opin. Chem. Biol.* **2001**, *5*, 724.
(42) (a) Schöneboom, J. C. Combined Quantum Mechanical/Molecular Mchanical Calculations on Cytochrome P450$_{cam}$. Ph.D. Thesis, The Heinrich-Heine University of Düsseldorf, Düsseldorf, Germany, 2003. (b) Cohen, S. Combined Quantum Mechanical/Molecular Mchanical Calculations on Reactivity and Structure of the Enzyme Cytochrome P450$_{cam}$. Part of a Ph.D. Thesis, The Hebrew University, Jerusalem, Israel.
(43) Melander, L.; Saunders, W. H., Jr. *Reaction rates of isotopic molecules*; Robert E. Krieger Publishing Company: Malabar, FL, 1987.

semiclassical model uses Eyring's eq 1 for the reaction rate constant k_r as a function of temperature T. The function is dependent on the free energy of activation ($\Delta G^{\ddagger}$), R is the gas constant, and A is the frequency of passing through the transition state (given by RT/Nh, N being Avogadro's number and h Planck's constant).

$$k_r = A \exp(-\Delta G^{\ddagger}/RT) \quad (1)$$

Based on this equation, the semiclassical KIE becomes eq 2.

$$k_H/k_D = \exp[(\Delta G^{\ddagger}_D - \Delta G^{\ddagger}_H)/RT] \quad (2)$$

The other two models involve tunneling correction. Tunneling correction to the semiclassical KIE can be achieved by multiplying the Eyring KIE with the tunneling ratio ($Q_{t,H}/Q_{t,D}$). In the simplest model, Q_t is estimated from the Wigner correction in eq 3.[43]

$$Q_t = 1 + u_t^2/24 \text{ with } u_t = h\nu/k_B T \quad (3)$$

Here, h is Planck's constant, k_B is the Boltzmann constant, and ν is the value of the imaginary frequency in the transition state. An alternative tunneling correction is due to Bell, in eq 4:[43]

$$Q_t = Q_1 + Q_2$$

$$Q_1 = \frac{0.5u_t}{\sin(0.5u_t)}$$

$$Q_2 = -\sum_{n=1}^{\infty}(-1)^n \frac{\exp\dfrac{(u_t - 2n\pi)\Delta E^{\ddagger}}{u_t}}{\dfrac{u_t - 2n\pi}{u_t}} \quad (4)$$

3. Results

Scheme 4 summarizes the key species characterized in this study, using Cpd I and the probe substrate, *trans*-2-phenylmethyl cyclopropane, **1**. The hydroxylation process follows a rebound[2−6] mechanism with a radical complex intermediate, $\mathbf{I}_U$, formed via a hydrogen abstraction transition state, $\mathbf{TS}_H$. Rebound of the radical leads to the alcohol complex of the unrearranged (*U*) product, **2**, via the rebound transition state $\mathbf{TS}_{reb}(U)$. The radical may also rearrange via $\mathbf{TS}_R$ leading initially to the rearranged radical complex, $\mathbf{I}_R$, and subsequently to the rearranged product complex, **3**. In addition to $\mathbf{I}_U$, we attempted to generate the corresponding cationic complex, "$\mathbf{I}_U{}^+$", by shifting the electron from the radical center to the heme moiety. However, as we shall discuss later, this is not really a cationic species, either for substrate **1** or for **4**, and hence it is shown in the scheme in inverted commas and a question mark. Most of the species appear in two spin varieties, LS (doublet) and HS (quartet). The following text keeps making use of these labels of the critical species for hydroxylation of the probe substrates **1** and **4**.

3.A. Reaction Profile for Hydroxylation of 1 Without Skeletal Rearrangement. Figure 1 displays the B3LYP/LACVP computed reaction profile for hydroxylation of **1** leading to the unrearranged alcohol complex. The energy data within parentheses involve zero-point energy correction, while the data in brackets are obtained by single-point calculations at the B3LYP/LACV3P^{+}* level. Much like all previous studies of C−H hydroxylation,[25,32] the Newcomb probe too exhibits a two-phasic mechanism, first hydrogen abstraction and then radical rebound.

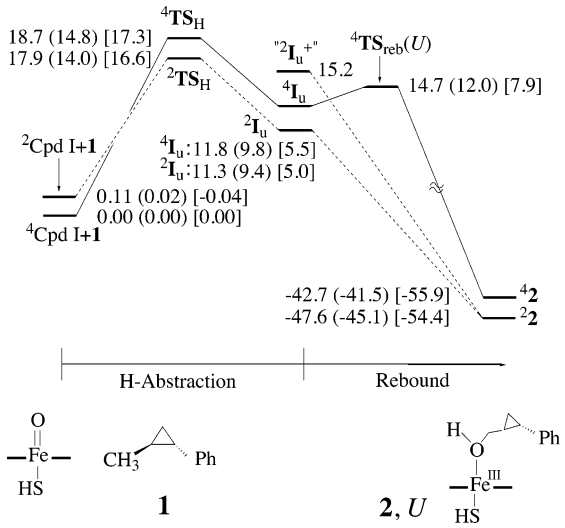

Figure 1. LACVP energy profiles (in kcal/mol) for the high-spin and low-spin hydroxylation of **1**, leading to the unrearranged alcohol complex, **2**. For each species, we show three energy values, which are relative energy (out of parentheses), relative energy with ZPE correction (within parentheses), and relative LACV3P^{+}* energy (within square brackets).

Another similarity is the doubling of the profiles to closely lying HS and LS mechanisms nascent from the two spin states of Cpd I. It is seen that throughout the hydrogen abstraction phase the two profiles are close within less than 1 kcal/mol. In the rebound phase, HS and LS bifurcate: the HS radical complex ($^4\mathbf{I}_U$) encounters a barrier for rebound via $^4\mathbf{TS}_{reb}(U)$, while the LS species ($^2\mathbf{I}_U$) behaves as a shoulder on the potential energy surface and falls in a barrierless fashion to the corresponding low-spin ferric alcohol complex, ^{2}**2**. The third intermediate "$^2\mathbf{I}_U{}^+$" is obtained by shifting the radical from the carbinyl group to the heme and letting the so generated species optimize its electronic structure. While this species is discussed later on in more detail, here suffices it to mention that "$^2\mathbf{I}_U{}^+$", too, rebounds spontaneously to give the LS ferric alcohol complex (see scan in the Supporting Information).

The larger basis set hardly changes anything during the hydrogen abstraction phase but stabilizes the radical complex intermediates, $^{4,2}\mathbf{I}_U$, as well as the product complexes, ^{4,2}**2**, and inverts the relative stability of the latter. Clearly, the Newcomb probe is hydroxylated, according to theory, by a two-state rebound mechanism similar to other substrates studied thus far.[25,29,32]

Figure 2 shows the key geometric features and spin densities for the hydrogen abstraction phase. The porphyrin, which had a significant spin density in Cpd I, loses most of its spin in $^{4,2}\mathbf{TS}_H$, while at the same time the radical moiety acquires significant spin density. Structurally, the $^{4,2}\mathbf{TS}_H$ species involve C−H activation and some skeletal changes in the cyclopropyl carbinyl moiety that respond to the C−H activation by stabilizing the developing radical center on C_1. These features are very similar to the previously studied cases.[25,29,32] There is, however, a key difference; for the present case, the HS species is significantly more advanced compared with the LS. In the language of physical organic chemistry,[43] the latter transition state is virtually "central", with very similar O- - -H and C- - -H bond lengths (virtually identical bond orders), while the HS species is "late" with a long C- - -H bond (small bond order) and short O- - -H (large bond order). This is evident also from

^{4}**TS**$_H$ (^{2}**TS**$_H$)

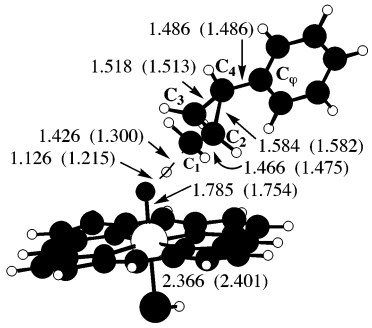

$\angle OHC_1$ = 169.9 (174.8)

ω_{Im} = *i*934.6 (*i*1000.2) cm^{-1}

	ρ_{Fe}	ρ_O	ρ_H	ρ_{Por}	ρ_{SH}	ρ_{Alk}
HS	1.60	0.60	-0.02	-0.06	0.17	0.71
LS	1.78	0.00	0.02	-0.18	-0.11	-0.52

Figure 2. LACVP optimized geometries (Å and degrees) of the hydrogen abstraction transition states (^{4,2}TS$_H$) for probe substrate **1**. Group spin densities (ρ) are noted below the drawing; HS corresponds to high-spin and LS to low-spin.

the spin distribution, which shows almost a fully developed spin on the radical moiety in ^{4}**TS**$_H$ and less so in ^{2}**TS**$_H$.

The species involved in the rebound phase are depicted in Figure 3, along with their corresponding spin density distributions. The radical complexes, ^{2}**I**$_U$ and ^{4}**I**$_U$, appear very similar, with the exception of their distance to the hydroxo group, which is longer for the HS species. In both cases, the C_2-C_4 bond of the cyclopropyl moiety is elongated considerably to stabilize the radical on C_1. As discussed above, only the HS complex encounters a barrier for rebound, via a transition state which is shown in the figure along with the value of the imaginary frequency.[25,32] The ^{4}**TS**$_{reb}$(*U*) species displays the expected changes vis-à-vis the corresponding radical complex; the Fe−O and Fe−S bonds elongate, and spin density lost by the radical is shifted to the iron center. The ferric alcohol complexes of the unrearranged product show all the expected features, longer Fe−O and Fe−S bonds for the HS complex due to the population of the $\sigma^*(d_{z^2})$ orbital which is antibonding along the S−Fe−O axis.

3.B. Reaction Profile for the Skeletal Rearrangement of the HS and LS Radical Complexes. Figure 4 displays the rearrangement energy profile starting from ^{4,2}**I**$_U$. The corresponding transition states are shown too, and the barriers are of the order of 1 kcal/mol for the two spin states, slightly lower than the barrier of the free radical; the latter is indicated in Figure 3 as $\Delta E_{free}^{\ddagger}$. Thus, complexation of the radical does not significantly change its barrier for rearrangement, and in the absence of any steric constraints in the protein pocket, this justifies the use of free radical data[13,15] to discuss the rearrangement process. Another feature is that the rearranged radical complexes, ^{4,2}**I**$_R$, are significantly more stable than the unrearranged species, which means that the rearrangement is not a reversible process. The ^{4,2}**TS**$_R$ species exhibit the expected skeletal rearrangement, C_2-C_4 elongation and C_1-C_2 shortening. The LS transition state appears to be somewhat more advanced than the HS counterpart, as may be evidenced from the shorter C_1-C_2 distance and the greater accumulation of spin density on C_4, the α-to-phenyl position.

Figure 5 depicts the reaction profile for the rebound process of the rearranged radical complexes, while Figure 6 shows the corresponding critical species. The LS counterpart in Figure 5 is a virtual process, since the unrearranged radical, ^{2}**I**$_U$, has no barrier for rebound (see Figure 1), and hence it will form only the unrearranged alcohol complex and *will not populate* the ^{2}**I**$_R$ species (although it may be slightly populated at the expense of ^{4}**I**$_R$ via spin crossover). Nevertheless, we depict both HS and LS processes, since *this is the first case that exhibits a rebound barrier and a genuine transition state species on the LS manifold*. The origins of the LS rebound barrier here are apparent from the spin density data in the **I**$_R$ species in Figure 6. Both species involve a benzylic radical moiety with spin density significantly delocalized into the benzene ring. As such, the rebound is attended by loss of the resonance energy of the radical moiety, and this loss is in the roots of the rebound barrier on both spin manifolds. The LS barrier is also curiously higher than the HS barrier, and the reason for that coincides precisely with the steric requirements for rebound in the two spin manifolds. This can be understood based on previous descriptions of the rebound process.[25,27,44] During HS rebound, the unpaired electron shifts from the radical to the iron, to populate the $\sigma^*(d_{z^2})$ orbital which is oriented along the S−Fe−O axis. The overlap requirement of the radical with the accepting orbital allows the organic substrate in ^{4}**TS**$_{reb}$(*R*) to assume a sterically convenient orientation above the porphyrin plane, as can be judged from the angles $\angle FeOC_4 = 168°$ and $\angle OC_4C_3 = 91°$. By contrast, during LS rebound the unpaired electron shifts from the radicals to the $\pi^*(d_{xz})$ orbital, which ideally would require an $\angle FeOC_4$ angle of 100−110° or so, which is impossible in the present system due to severe steric repulsion between the radical moiety and the porphyrin. As such, the LS rebound process settles for a compromise geometry that releases the steric repulsion by assuming an $\angle FeOC_4$ angle of 161°. However, at this angle the overlap with the accepting orbital, $\pi^*(d_{xz})$, is drastically weakened and so is the C_4- - -O bonding. Some traces of this repulsion are still present however, as may be judged from the $\angle OC_4C_3$ angle of 83°, which shows the inherent propensity of the radical to incline in order to maximize the overlap with the accepting orbital, $\pi^*(d_{xz})$.

3.C. Kinetic Isotope Effects in the Reactions of Probe Substrate 1. Table 1 collects the calculated kinetic isotope effect (KIE) data for the hydrogen abstraction phase of **1** at two temperatures, the latter 303 K being the experimental temperature.[30] Each entry has three different KIEs, corresponding to semiclassical (I) and tunneling-corrected (II, III) values. To test whether the KIEs are determined by the zero-point energy (ZPE) or by the thermal factors, we display also the KIEs calculated with ZPE only. The first two entries in the table correspond to the intramolecular isotope effect, e.g., in entry 1, the KIEs refer to hydrogen or deuterium abstraction from the dideuterated substrate, **1**-D_2H. The rest of the entries correspond to intermolecular isotope effects calculated for the indicated isotopically substituted substrates. It is seen that generally KIE(HS) < KIE(LS) and that this trend is determined by the ZPE contributions

(44) Harris, N.; Cohen, S.; Filatov, M.; Ogliaro, F. *Angew. Chem., Int. Ed.* **2000**, *39*, 2003−2007.

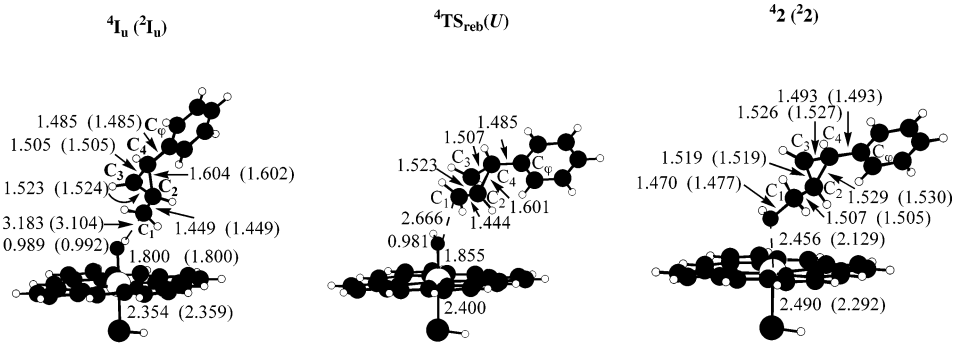

	ρ_{Fe}	ρ_{OH}	ρ_{por}	ρ_{SH}	ρ_{Alk}
HS	1.80	0.32	-0.12	0.04	0.96
LS	1.80	0.25	-0.12	0.01	-0.94

ρ_{Fe}	ρ_{OH}	ρ_{por}	ρ_{SH}	ρ_{Alk}
2.09	0.12	-0.13	0.08	0.84

	ρ_{Fe}	ρ_{OH}	ρ_{por}	ρ_{SH}	ρ_{Alk}
HS	2.57	0.02	-0.03	0.44	0.00
LS	1.10	0.00	-0.09	-0.01	0.00

Figure 3. LACVP optimized geometries (Å and degrees) of the species involved in the rebound phase of Figure 1.

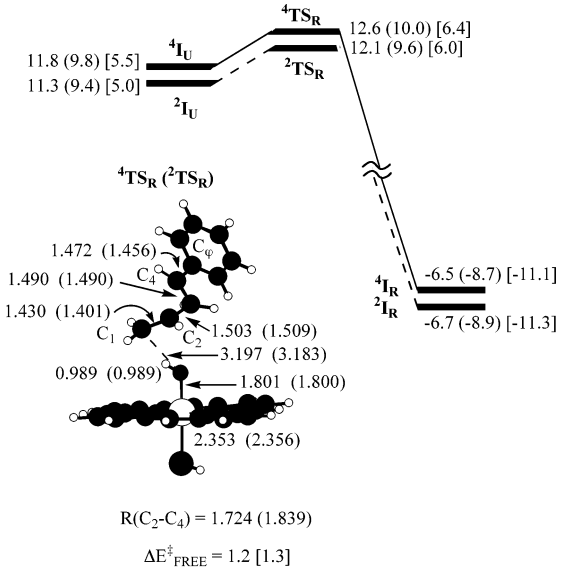

	ρ_{Fe}	ρ_{OH}	ρ_{por}	ρ_{SH}	ρ_{C1}	$\rho_{C2\text{-}C3}$	ρ_{C4}	$\rho_{C\varphi}$
HS	1.79	0.31	-0.12	0.06	0.75	-0.12	0.27	0.06
LS	1.79	0.27	-0.13	0.03	-0.60	0.16	-0.41	0.11

Figure 4. LACVP energy profiles (in kcal/mol) for the rearrangement of the HS and LS radical complexes intermediates, $^{4,2}\mathbf{I}_U$, to the rearranged ones, $^{4,2}\mathbf{I}_R$. The relative energy data follow the same order specified in Figure 1. The geometric features and spin densities (ρ) of the rearrangement transition states ($^{4,2}TS_R$) are shown below the energy profiles. $\Delta E^{\ddagger}_{free}$ is the rearrangement barrier of the free radical (LACVP datum out of brackets and LACV3P^{+*} in brackets).

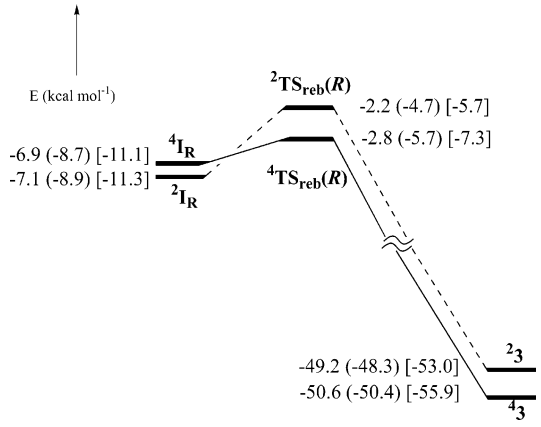

Figure 5. LACVP energy profiles (in kcal/mol) for the rebound processes of the rearranged radical complexes, $^{4,2}\mathbf{I}_R$, which lead to the rearranged alcohol complex $^{4,2}\mathbf{3}$. The relative energy data follow the same order specified in Figure 1.

to the respective HS and LS processes. In the last entry, the intermolecular KIE, **1**-H_3/**1**-D_3, exhibits an opposite trend for the classical and Wigner corrected values, but the trend KIE(HS) < KIE(LS) is obtained with Bell tunneling correction.

Table 2 displays the corresponding KIE values for allylic hydroxylation of propene[32] by two different Cpd I models, one representing P450 and the other having instead a thiolate or an imidazole (ImH) ligand. It is seen that irrespective of the Cpd I species, the isotopic substitution pattern, and the inclusion or omission of tunneling correction, here KIE(HS) > KIE(LS). The comparison of Tables 1 and 2 shows that, in each case, the kinetic isotope effects for the HS and LS processes are different, i.e., KIE(HS) ≠ KIE(LS), and that the relative isotopic sensitivity depends on the substrate undergoing C−H cleavage. As we shall discuss later, these trends derive from the different structures of the corresponding $^{4,2}\mathbf{TS}_H$ species for hydrogen abstraction (e.g., Figures 1 and 2) and from the dependence of these differences on the substrate.

3.D. Reaction Profile for Hydroxylation of the Substrate Probe 4. Figure 7 displays the reaction profile for the hydroxylation of **4** (see **4** in Scheme 3). It is seen that for this substrate the profile involves effectively concerted hydroxylation mechanisms in both the LS and the HS manifold. The transformation of the HS mechanism, for this substrate, from a stepwise one, with a barrier for rebound, to an effectively concerted one was predicted before based on analysis of the factors that control the rebound barrier.[25,27,44] The transition states $^{2,4}TS_H$ and $^{2,4}\mathbf{I}_U$ species are shown in Figure 8, along with the charge (Q) and spin (ρ) density distributions on the alkyl moiety. The transition states are shown to correspond to hydrogen abstraction species, having no unusual features other than very large imaginary frequencies that may reflect that the transition state mode motion occurs under a sterically constrained potential, due to the dimethyl moiety that flanks the hydrogen in transit. The $^{2,4}\mathbf{I}_U$ species in Figure 8 correspond to the usual iron−hydroxo/alkyl

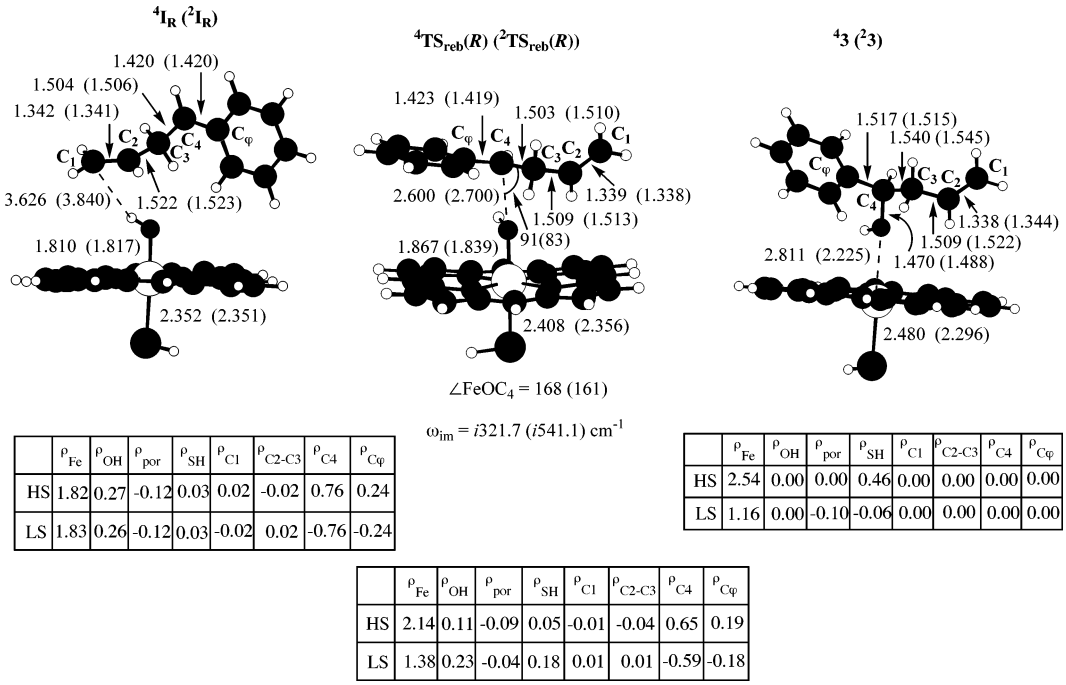

	ρ$_{Fe}$	ρ$_{OH}$	ρ$_{por}$	ρ$_{SH}$	ρ$_{C1}$	ρ$_{C2-C3}$	ρ$_{C4}$	ρ$_{Cφ}$
HS	1.82	0.27	-0.12	0.03	0.02	-0.02	0.76	0.24
LS	1.83	0.26	-0.12	0.03	-0.02	0.02	-0.76	-0.24

	ρ$_{Fe}$	ρ$_{OH}$	ρ$_{por}$	ρ$_{SH}$	ρ$_{C1}$	ρ$_{C2-C3}$	ρ$_{C4}$	ρ$_{Cφ}$
HS	2.54	0.00	0.00	0.46	0.00	0.00	0.00	0.00
LS	1.16	0.00	-0.10	-0.06	0.00	0.00	0.00	0.00

	ρ$_{Fe}$	ρ$_{OH}$	ρ$_{por}$	ρ$_{SH}$	ρ$_{C1}$	ρ$_{C2-C3}$	ρ$_{C4}$	ρ$_{Cφ}$
HS	2.14	0.11	-0.09	0.05	-0.01	-0.04	0.65	0.19
LS	1.38	0.23	-0.04	0.18	0.01	0.01	-0.59	-0.18

Figure 6. LACVP geometries (Å and degrees) and group spin densities for the species participating in the rebound processes of the rearranged radical complexes, ^{4,2}**I**$_R$, described in Figure 5.

Table 1. Computed Kinetic Isotope Effects (*KIE*s) in the Hydrogen Abstraction Phase for **1** + ^{4,2}**Cpd I**

			T = 298 (303) K		T = 298 K, ZPE[b]	
entry	isotopic substitution	*KIE* model[a]	LS	HS	LS	HS
		I	6.20 (6.02)	5.72 (5.07)	5.86	5.35
1	**1**−CHD-H/**1**−CH$_2$−D[c]	II	7.63 (7.37)	6.86 (6.06)	7.23	6.42
		III	10.91 (10.28)	8.92 (7.75)	10.46	8.35
		I	5.66 (6.04)	5.77 (5.61)	6.02	5.47
2	**1**−CD$_2$−H/**1**−CHD−D	II	6.94 (7.37)	6.89 (6.67)	7.35	6.53
		III	9.74 (10.08)	8.84 (8.42)	10.27	8.38
		I	6.69 (6.49)	6.49 (6.30)	6.09	5.90
3	**1**−CH$_2$−H/**1**−CH$_2$−D	II	8.35 (8.07)	7.84 (7.58)	7.60	7.12
		III	12.45 (11.70)	10.36 (9.84)	11.33	9.41
		I	6.22 (6.04)	5.77 (5.61)	5.75	4.93
4	**1**−CD$_2$−H/**1**−CH$_2$−D	II	7.65 (7.37)	6.87 (6.68)	6.98	5.86
		III	10.70 (10.09)	8.83 (8.41)	9.67	7.43
		I	8.06 (7.81)	8.55 (8.27)	6.81	7.43
5	**1**−CH$_2$−H/**1**−CD$_2$−D[d]	II	10.24 (9.84)	10.43 (10.01)	8.64	9.05
		III	15.56 (14.53)	13.85 (13.15)	13.11	12.05

[a] Based on eqs 2−4: I = semiclassical, II = Wigner correction, III = Bell correction. [b] Using $\Delta E^{\ddagger}$ + ZPE instead of $\Delta G^{\ddagger}$ in equations. 2−4. [c] $KIE_{reb}(U)$ = 1.09; KIE_R = 1.01 (HS,LS). [d] $KIE_{reb}(U)$ = 0.99; KIE_R = 0.98 (HS,LS).

radical complexes having virtually complete radical development on the alkyl moiety.

As already noted, the ^{2,4}**I**$_U$, species behave as shoulders on the potential energy surface and once the alkyl radical snaps out of the weak OH- - -C interaction (see Figure 8), the subsequent rebound process is barrierless. The electronic reorganization along the rebound pathway is very instructive and can be deduced from Figure 9, which plots the charge on the alkyl group along the rebound path for the HS process. It is seen that initially close to the ^{4}**I**$_U$, species, where the C- - -O distance is long, the charge on the alkyl group is small (∼0.1). As the C- - -O distance shortens the charge rises quite fast to 0.55 and then drops. Precisely, the same observation holds true for the LS rebound process, but the carbocationic development starts earlier in the corresponding LS process. Thus, as we noted originally,[25,27,44] the rebound process involves, concomitantly with C−O bond making, a single electron transfer from the alkyl radical to the iron−hydroxo complex. In other terms, there is a crossover and mixing of the valence forms PorFeOH/Alk• and

Table 2. *KIE* in the Hydrogen Abstraction Phase for Allylic Hydroxylation of Propene at *T* = 298 K

			Cpd I (SH$^-$)[c]		Cpd I (ImH)[d]	
entry	isotopic[a] substitution	*KIE*[b] model	LS	HS	LS	HS
1	CD$_2$−H/CDH−D	I	5.39	6.28	4.83	6.22
		II	6.67	9.28	5.40	9.05
2	CHD−H/CH$_2$−D	I	5.30	6.16	4.56	5.96
		II	6.56	9.11	5.10	8.65
3	CD$_2$−H/CH$_2$−D	I	5.24	6.09	4.54	5.89
		II	6.39	8.92	4.97	8.46
4	CH$_2$−H/CD$_2$−D	I	5.93	7.01	5.40	7.03
		II	7.66	10.61	6.46	10.56

[a] Refers to the allylic CH$_3$ group in H$_2$C═CHCH$_3$. [b] Based on eqs 2−4; I = semiclassical, II = Wigner corrected values. [c] Using Cpd I model for P450 from reference 32. [d] Using Cpd I with an imidazole ligand (unpublished data by our group).

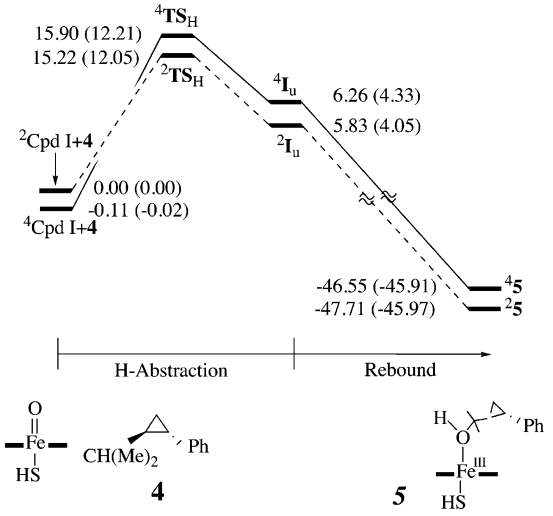

Figure 7. LACVP energy profiles (kcal/mol) for the high-spin and low-spin hydroxylation of **4**, leading to the unrearranged alcohol complex, **5**. For each species we show two energy values: relative energy (out of parentheses), relative energy with ZPE correction (within parentheses).

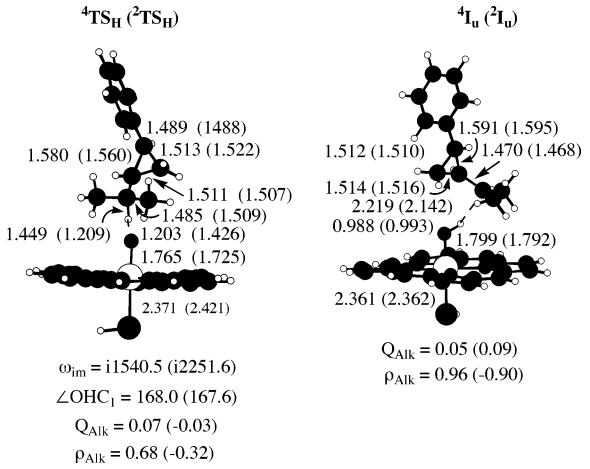

Figure 8. LACVP optimized geometries (Å and degrees) of the hydrogen abstraction transition states ($^{4,2}TS_H$) and intermediate radical complexes ($^{4,2}I_U$) for probe substrate **4**. Group spin densities (ρ) and charges (Q) on the alkyl moiety are noted below the drawing. C_1 is the radical center.

PorFeOH($^-$)/Alk$^+$ during the rebound. This crossover was verified by computational means by calculating the carbocationic form at the geometry of the radical and letting it optimize its geometry (see Supporting Information).

The so optimized PorFeOH($^-$)/Alk$^+$ LS species, nascent from probe substrates **1** and **4**, are depicted in Figure 10 and labeled as "$^2I_U(4)^+$" and "$^2I_U(1)^+$". For "$^2I_U(4)^+$", we were unable to locate a true cationic minimum; the optimized "$^2I_U(4)^+$" species has two imaginary frequencies, the major one being the rebound mode indicating that "$^2I_U(4)^+$" is a species downhill the rebound process en route to the ferric alcohol complex. Nevertheless, we show the species since its features can serve to illustrate the changes in electronic structure as the substrate is varied from **1** to **4**. Inspection of the charge on the radical moiety, Q_{Alk}, shows that "$^2I_U(1)^+$" is not a cationic species, even under the influence of a polarizing medium with a dielectric constant $\epsilon = 5.7$. By contrast, $^2I_U(4)^+$, which has clearly a significant positive charge and very little spin density on the organic moiety, is more clearly cationic in nature. However, this species too is not a free cation but rather a tight ion pair species with a significantly delocalized nature, very much reminiscent of our finding for the "cationic" σ-complex during benzene hydroxylation.[34]

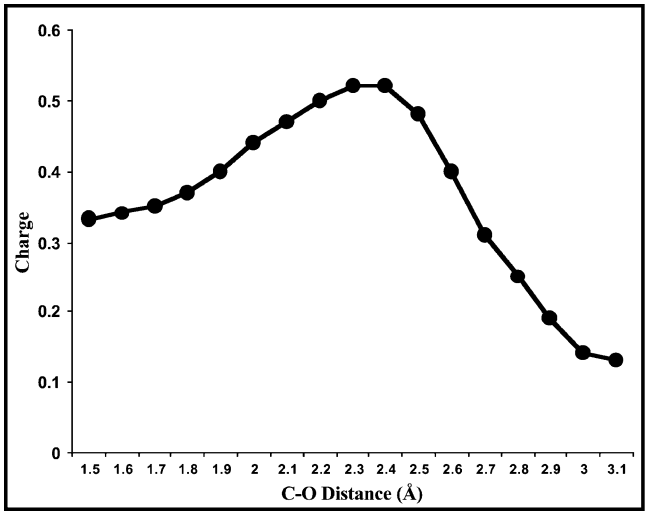

Figure 9. LACVP calculated charges on the alkyl moiety during the high-spin rebound pathway for probe **4**. A similar plot applies also to the low-spin rebound pathway of **4**.

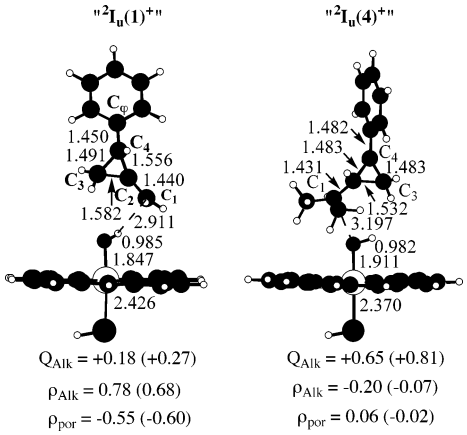

Figure 10. LACVP optimized geometries (Å and degrees) of "$^2I_U(1)$" (see Figure 1) and "$^2I_U(4)$" along with some group charges and spin densities. "$^2I_U(4)$" is a species downhill the rebound process shown in Figure 7.

4. Discussion

4.A. Two-State Reactivity Patterns in the Hydroxylation of Probe Substrates 1 and 4. Figures 1−3 show that *trans*-2-phenyl-methyl cyclopropane (**1**) is hydroxylated in a two-state reactivity (TSR) scenario.[25−27] Since the $^{2,4}TS_H$ species are higher in energy than all the successive species, the rate-determining step will be the hydrogen abstraction. To assess the behaviors of the two states, we collected in Table 3 the computed data on the effect of polarity and NH- - -S hydrogen bonding on the critical species that participate in the hydrogen abstraction phase and the rebound-rearrangement phases. It is seen that the LS transition state for the hydrogen abstraction phase is lower than the corresponding HS species. The polarity and hydrogen bonding to thiolate exert opposing effects on the relative energies, so that the combination of both factors leave the energy difference of the TSs almost unchanged, close to 1 kcal/mol. Thus, under the assumption that the relative abundance of the two states will be determined by the relative energy of the two transition state species, then the calculations predict a preponderance of the LS pathway over the HS counterpart by

Table 3. Effect of Medium Polarity (Represented by a Dielectric Constant, ϵ) and Hydrogen Bonding to Thiolate on a Few Species Located in the Study of C−H Hydroxylation of **1**[a]

entry	species	$\epsilon = 1$	$\epsilon = 5.7$	2NH- - -S	$\epsilon = 5.7$ +2NH- - -S
1	^{4}**TS**$_H$	0.0	0.0	0.0	0.0
2	^{4}**I**$_U$	−6.9	−5.8	−7.2	−6.1
3	^{4}**TS**$_{reb}$(*U*)	−4.1	−3.8	−5.6	−4.6
4	^{4}**TS**$_R$	−6.0	−4.6	−6.5	−4.9
5	^{2}**TS**$_H$	−1.1; −0.8[b]	−1.8	+0.3	−0.7 (−0.7[c])
6	^{2}**I**$_U$	−7.4	−6.2	−7.9	−6.8
7	^{2}**TS**$_R$	−6.6	−5.4	−6.5	−5.5

[a] All values are in kcal/mol and obtained with JAGUAR 4.1. The labels of the species follow Scheme 4 and Figures 1−4. [b] This datum is obtained with GAUSSIAN. [c] Calibrated with ZPE correction.

Scheme 5. Qualitative Representation of the Calculated Rebound and Rearrangement Processes for the Unrearranged Radical Complexes ^{4,2}**I**$_u$ of **1**[a]

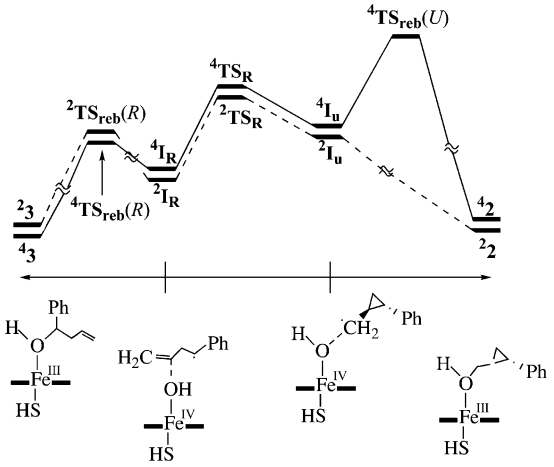

[a] Note the relative rearrangement and rebound barriers for the HS ^{4}**I**$_u$ species vs. the LS one, ^{2}**I**$_u$.

roughly a factor of 3:1. Since the ^{2,4}**I**$_U$ species retain about the same energy difference, we might expect this 3:1 ratio to be conserved and continue onward to the other phases of the reaction.

Scheme 5 uses the data in Table 3 to illustrate *qualitatively* the competition of rebound (reb) and rearrangement (R) processes for the ^{2,4}**I**$_U$ species. Qualitatively speaking, the LS species has no barrier for rebound but has a finite barrier for rearrangement. As such, most, if not all, of the ^{2}**I**$_U$ species will proceed to the unrearranged product complex, ^{2}**2**, to produce the unrearranged alcohol byproduct release. By contrast, the ^{4}**I**$_U$ species encounters two barriers, but now, the higher one is for rebound. Consequently, most of the HS intermediate will proceed by radical rearrangement to give the ^{4}**I**$_R$ species, which subsequently yields the rearranged alcohol product, **3**. It follows therefore that at the limit where the LS path yields only **2** while the HS yields only **3**, the ratio [**2**,*U*/**3**,*R*] is simply the relative yield of the HS and LS processes in the total reaction yield. This ratio, therefore, does not strictly reflect the radical lifetime. Our theoretical estimate of this quantity is roughly 3:1, whereas experimental estimates are in the range of (3−10):1 depending on the P450 isoform and the chirality of **1**.[15−18,30] Of course, we do not even pretend that the calculations should reproduce precisely the experimental relative yield, because they do not take into account the variable polarity, hydrogen bonding capability, and topography of the protein pocket. Still, it is gratifying that theory can at least predict a significant yield of the rearranged product, in accord with experiment.[15−18,30]

The TSR scenario of probe substrate **4** in Figure 7 is extremely simple. Now both the LS and HS mechanisms are effectively concerted all the way to the ferric-alcohol products ^{2,4}**5**. This lack of rebound barrier has been predicted before,[25,27,44] based on analysis of the factors that determine the height of the HS barrier for rebound. Thus, it was predicted that as the radical center becomes a better electron donor (lower ionization energy), the rebound barrier will gradually decrease and at some limiting donor capability the barrier will altogether vanish. This prediction and the computational result match the experimental observation that **4** gave no detectable rearranged products.[15]

4.B. TSR Interpretation of Intrinsic Product Isotope Effect and Its Mechanistic Significance in the Hydroxylation of Probe Substrate 1. We recall the finding of Newcomb et al.[30] that the two products **2** and **3** exhibit different sensitivities to isotopic substitution of the scissile C−H bond in the substrate, **1**, such that the reaction is characterized by the product isotope effect (PIE) that is significantly different from unity, namely PIE(**2**,*U*/**3**,*R*) > 1. *This finding means by itself that **2** and **3** cannot be formed from a single intermediate that partitions into **2** and **3***; the finding requires two different mechanisms, and the applicability of TSR is examined and qualified in this section.

It is quite tricky to compare theoretical KIE values to experimentally determined ones, since the latter may be masked and may not reflect the intrinsic KIE value.[14,45] Jones and coworkers[14a] showed that, in a mechanism that branches into two products via two enzyme (Cpd I)−substrate (ES) complexes, the observed KIE will depend inter alia on the interconversion dynamics between the ES complexes, on the rate of dissociation of these complexes, and on rates of other processes which branch out from these complexes.[46a] In the TSR scenario, these factors would be the exchange rate of the HS and LS ES complexes, the rearrangement and rebound rate constants for the radical intermediate on the HS manifold, as well as other processes that may branch out from the ES complexes (e.g. an oxidase process and phenyl oxidation). Since the isotope effects for the rebound and rearrangement steps of the HS species for probe substrate **1** are close to unity (footnotes c and d, Table 1), we can overlook their effect.[31,33,46b] In addition, since the barrier data show that practically the HS path will not contribute to the unrearranged product, **2**, this simplified the treatment, and

(45) (a) Guengerich, F. P.; Calcutt, M. W.; Krauser, J. A.; Miller, G. P.; Martin, M. V.; Hanna, I. H.; Sato, I. *Rate-Limiting Steps in Cytochrome P450*, presented during the 13th International Conference on Cytochrome P450, Prague, The Czech Republic, June 28−July 3, 2003. (b) Jones, J. P.; Korzekwa, K. R.; Rettie, A. E.; Trager, W. F. *J. Am. Chem. Soc.* **1986**, *108*, 7074−7078.

(46) (a) The equation for the observed kinetic isotope effect (KIE_{obsv}) in ref 14a is the following: $KIE_{obs} = KIE_{int}\{[ES_H]/[ES_D]\} = [KIE_{int}(k_2 + 2k_r) + k_H]/[(k_2 + 2k_r) + k_H]$. It corresponds to a case where a substrate has two isotopically distinct but chemical equivalent sites, e.g., *p*-xylene with one CD_3 group. KIE_{int} in the equation is the intrinsic isotope effect, ES is the enzyme−substrate complex, and $[ES_H/ES_D]$ is the ratio of the concentrations of the protio and deuterio complexes. The latter ratio depends also on their rate of exchange of the two isotopic sites (k_r), the rate of dissociation of the ES complex (k_2), and the rate constant of C−H hydroxylation. Any other process that branches out from the ES complexes will further affect the expression by changing selectively the concentrations of the protio and/or deuterio ES complexes. (b) In the previous studies,[31,33] we derived an expression which was based on the assumption that the HS and LS complexes are either in fast equilibrium or leading to two disconnected processes. For this case, we obtained the following expression for the product isotope effect: $PIE(\mathbf{2}/\mathbf{3}) = [\mathbf{2}_H/\mathbf{2}_D]/[\mathbf{3}_H/\mathbf{3}_D] = (KIE_{LS}/KIE_{HS})\cdot\Phi$, where the function Φ incorporates the isotopic dependence of the rearrangement and rebound steps in the HS manifold; i.e, $\Phi = \{(1/KIE_R)\text{-}[(k_R^H/k_{reb}^D + KIE_{reb}(U))]/[(k_R^D/k_{reb}^D) + 1]\}$. The calculations show that Φ is virtually unity.

the derivation of Jones et al.[14a] can be used to write the following expression for the observed product isotope effect, PIE-$(\mathbf{2}/\mathbf{3})_{obs}$:[14a]

$$PIE(\mathbf{2}/\mathbf{3})_{obs} = [\mathbf{2}_H/\mathbf{2}_D]/[\mathbf{3}_H/\mathbf{3}_D] = (KIE_{\mathbf{LS}}/KIE_{\mathbf{HS}})\cdot\{([ES_H]/[ES_D])_{\mathbf{LS}}/([ES_H]/[ES_D])_{\mathbf{HS}}\}$$

$$PIE(\mathbf{2}/\mathbf{3})_{int} \equiv PIE(\mathbf{2}/\mathbf{3})_{TSR} = (KIE_{LS}/KIE_{HS}) \quad (5)$$

The parenthetical term in eq 5 is the ratio of intrinsic isotope effects for C−H bond activation, in the LS and HS manifolds, $PIE(\mathbf{2}/\mathbf{3})_{int}$. The terms in wiggly brackets represent the concentrations of the ES complexes of the protio and deuterio varieties in the two spin manifolds. The equation predicts that, in a branching mechanism, like TSR, the quantity $PIE(\mathbf{2}/\mathbf{3})_{obs}$ will generally reflect an interplay of the intrinsic isotope effect ratio and the concentration of the ES complexes. In the general case, where both terms vary, an observation of $PIE(\mathbf{2}/\mathbf{3})_{obs}$ different than 1 will only mean that **2** and **3** cannot be formed from a single intermediate *but will not reveal other mechanistic information*.

Of particular interest to us here are those cases where PIE_{obs} is determined by the intrinsic isotope effects ratio. The analysis of Jones and co-workers[14a] shows two limiting situations where this will hold, under conditions of either (i) fast equilibration between the HS and LS complexes or (ii) slow exchange, when the rate of dissociation of the ES complex is faster than the rate of C−H activation. In these situations, the observed PIE will be given by the intrinsic PIE value and can be quantified from the kinetic isotope effects for the TSR scenario, as follows in eq 6:

$$PIE(\mathbf{2}/\mathbf{3})_{obs} \approx PIE(\mathbf{2}/\mathbf{3})_{int} = (KIE_{LS}/KIE_{HS});\ PIE(\mathbf{2}/\mathbf{3})_{int} = PIE(\mathbf{2}/\mathbf{3})_{TSR} \quad (6)$$

We have no precise knowledge about the rate of exchange of the ES complexes of the two spin varieties, but certainly for a nonpolar substrate like **1**, we may expect the rate of dissociation of the ES [(Cpd I)−substrate] complexes to be faster than the rate of C−H activation. Thus, eq 6 may be valid for the cases such as **1**-D_2H where the isotope effect is determined intramolecularly (where less masking is expected). Be this as it may, since theory can provide intrinsic PIE values, it would be interesting to compare them to the observed ones and then analyze the mechanistic significance of the intrinsic property.

Using the kinetic isotope effects data in Table 1 and eq 6, we calculated the intrinsic PIE quantities [given as $PIE(\mathbf{2}/\mathbf{3})_{TSR}$] that are shown in Table 4 alongside the experimental values, $PIE(\mathbf{2}/\mathbf{3})_{obs}$. The first two entries in Table 4 correspond to intramolecular KIEs, while the rest, to intermolecular values. It is seen that all the intramolecular values and the majority of the intermolecular ones lead to $PIE(\mathbf{2}/\mathbf{3})_{TSR}$ that is greater than unity. All in all, using intramolecular isotope effects, the calculated $PIE(\mathbf{2}/\mathbf{3})_{TSR}$ quantity behaves like the observed one; both predicting that the unrearranged product, **2**, should exhibit greater sensitivity to isotopic replacement compared with the rearranged product, **3**.

The less conclusive datum corresponds to the intermolecular isotope effect (**1**-H_3/**1**-D_3) in entry 5. Early experimental data

Table 4. Intrinsic and Observed Product Isotope Effects[a] in the Hydroxylation of **1**

entry	isotopic substitution	*T* (K)	$PIE(\mathbf{2}/\mathbf{3})_{TSR}$[a]	$PIE(\mathbf{2}/\mathbf{3})_{obs}$
1	**1**−CHD−H/**1**−CH_2−D	298	1.08 (1.11) [1.22]	1.14[b]
		303	1.19 (1.22) [1.33]	
2	**1**−CD_2−H/**1**−CHD−D	298	0.98[d] (1.01) [1.10]	
		303	1.08 (1.11) [1.20]	
3	**1**−CH_2−H/**1**−CH_2−D	298	1.03 (1.07) [1.20]	
		303	1.03 (1.07) [1.19]	
4	**1**−CD_2−H/**1**−CH_2−D	298	1.08 (1.11) [1.21]	
		303	1.08 (1.10) [1.20]	
5	**1**−CH_2−H/**1**−CD_2−D	298	0.94 (0.98) [1.12]	>1[c]
		303	0.95 (0.98) [1.11]	

[a] $PIE(\mathbf{2}/\mathbf{3})_{TSR}$ is identical to $PIE(\mathbf{2}/\mathbf{3})_{int}$, see eq 6. The datum out of parenthesis involves semiclassical KIE_s. The data in parentheses and square brackets include tunneling corrections using Wigner's (eq 3) and Bell's (eq 4) models, respectively. [b] An average of the experimental values in ref 30. [c] Only a direction, *PIE* > 1, is reported in ref 30. Attempts to determine the individual KIEs for **2** and **3** from the Supporting Information, of ref 30, led to some very low values, possibly indicative of masked KIEs. [d] With ZPE only, PIE = 1.10, See Table 1.

by Newcomb and Ingold[47] for the **1**-H_3 and **1**-D_3 isotopomers of *trans*-2-phenyl-methyl cyclopropane revealed values both smaller and larger than unity. By contrast, the more recent, and presumably more accurate, data of Newcomb et al.[30] indicate that the observed PIE value should be larger than unity, even though an actual PIE value was not determined. The PIE derived from TSR leads to a value larger than unity when Bell's tunneling correction is applied, but otherwise the value is smaller than or close to unity. Apparently, the intermolecular isotope effect is difficult to measure and is less reliable than intramolecular values due to masking effects and very small yields.[7,14,45] Hence the mismatch of the classical PIE_{int} value and the experimental one may reflect that the experimental isotope effects are not intrinsic values due to masking (see footnote c in Table 4). A factor that may affect the intrinsic isotope effect is phenyl hydroxylation, which was shown in a recent study to occur from the LS manifold.[34] As shown later, this reaction will become important for the **1**-H_3 and **1**-D_3 isotopomer, and only in the LS manifold. Thus, phenyl hydroxylation will selectively reduce the concentration of $[ES_D]_{\mathbf{LS}}$ in eq 5 and will produce a *PIE* value larger than unity. If the suppression of $[ES_D]_{\mathbf{LS}}$ is large, say by a factor ≫1, the observed *PIE* will be large and may exceed unity by a significant margin. Still though, the option of tunneling should not be discounted as a possible source of *PIE* > 1.[48]

To understand the mechanistic significance of the $PIE(\mathbf{2}/\mathbf{3})_{int}$ quantity, we refer back to the physical organic theory of kinetic hydrogen isotope effect, $KIE_{H/D}$. A semiclassical treatment of the problem shows that the $KIE_{H/D}$ in a series of related hydrogen abstractions should exhibit a bell shape and reflects the asymmetry of the A- - -H- - -B moiety of the TS. The maximum $KIE_{H/D}$ value is obtained for TSs that are centrally located along the H-transfer coordinate between the two heavy atoms, while early and late TSs are expected to possess smaller

(47) Atkinson, J. K.; Hollenberg, P. F.; Ingold, K. U.; Johnson, C. C.; Le Tadic, M. H.; Newcomb, M.; Putt, D. A. *Biochemistry* **1994**, *33*, 10630−10637.
(48) For the importance of tunneling in enzymatic processes, see: (a) Francisco, W. A.; Knapp, M. J.; Blackburn, N. J.; Klinman, J. P. *J. Am. Chem. Soc.* **2002**, *124*, 8194−8195. (b) Kohen, A.; Klinman, J. P. *Acc. Chem. Res.* **1998**, *31*, 397−404. (c) Jonsson, T.; Glickman, M. H.; Sun, S.; Klinman J. P. *J. Am. Chem. Soc.* **1996**, *118*, 10319−10320. (d) Knapp, M. J.; Kinmann, J. P. *Eur. J. Biochem.* **2002**, *269*, 3113−3121. (e) Carbene ring expansion was found recently to involve tunneling even at room temperature: Zuev, P. S.; Sheridan, R. S.; Albu, T. V.; Truhlar, D. G.; Hrovat, D. A.; Borden, W. T. *Science* **2003**, *299*, 867−870.

Scheme 6. Bond Orders in the Hydrogen Abstraction Transition States of **1** and of Propene (the Geometries for Propene Are Taken from Ref 32) and Corresponding Ratios of the Kinetic Isotope Effects (*KIE*) for the LS and HS Processes

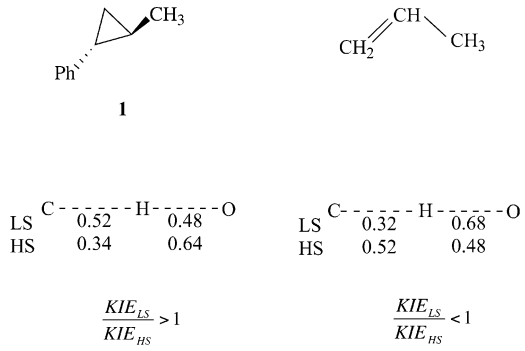

$KIE_{H/D}$ values.[49] While this is an oversimplified model for the P450 hydroxylation case (since the Fe═O has to be considered as well), still it is instructive to use it. Scheme 6 shows the bond orders of the C- - -H- - -O moieties of the hydrogen abstraction TSs for the reaction of **1** (see Figure 2) and for allylic hydroxylation of propene.[32] The bond orders (n) were calculated from the corresponding TS geometries, using the Pauling formula, $n = \exp[-(r^{\ddagger} - r^0)/a]$, and their sum was normalized to unity. Inspection of Scheme 6 shows that, in the case of **1**, the LS ^{2}**TS**$_H$ species is a "central" TS, while the corresponding HS species is a "late" species; these characters are fleshed out also from the spin densities on the alkyl moiety of the two species in Figure 2, as such, $KIE_{LS} > KIE_{HS}$, as revealed by the data in Table 1. By contrast, for allylic hydroxylation, the LS ^{2}**TS**$_H$ species is "late", while the corresponding HS species is "central", and hence the following relation holds: $KIE_{LS} < KIE_{HS}$ (Table 2). For probe substrate **4**, both transition states are not central, but ^{4}**TS**$_H$ is less distant from centrality than the ^{2}**TS**$_H$ species, and hence $KIE_{LS} < KIE_{HS}$ (see Table S.22). Based on eq 6, it *follows that the PIE(2/3)$_{int}$ quantity reflects inter alia the relative progression of the LS and HS transition states for hydrogen abstraction along the H-transfer coordinate* (C- - -H- - -O). While this argument is simplistic, it is nevertheless apparent that TSR predicts that the PIE_{int} quantity would generally be different than unity, since the HS and LS transition states have different geometries with different extents of C−H bond cleavage and O−H bond formation. Judging from the range of KIE_{LS} and KIE_{HS} values calculated for the present systems (**1**, propene, and **4**), which vary from a few percent up to 40%, one may expect a significant variation of the PIE_{int} quantity. PIE_{int} emerges in our view as a sensitive probe for the mechanism of C−H hydroxylation by P450 enzymes, in cases where intrinsic isotope effects can be determined. Any model aspiring to explain the mechanism will have to account for the PIE_{int} patterns, at least as well as TSR does.

4.C. TSR Interpretation of the Regioselectivity Reversal during Hydroxylation of the 1-D$_3$ Isotopomer. The foregoing results for C−H hydroxylation in **1** along with our previous calculations of benzene hydroxylation by P450[34] enable us to discuss the metabolic switching observed for the **1**-D_3 isotopomer of **1**.[47,50] Thus, while **1**-H_3 reacted mostly by C−H hydroxylation, with minor phenyl hydroxylation, the **1**-D_3 isotopomer exhibited predominant phenyl hydroxylation. This reversal of regiochemistry (metabolic switching) indicates that the barriers for the two processes are very close, so that isotopic substitution can tip the balance. Let us see whether a reactivity scenario invoking only Cpd I can account for these observations.

Scheme 7. Comparison of an Estimated Barrier (kcal/mol) for Phenyl Hydroxylation of **1** with the Calculated Hydrogen Abstraction Barriers for C−H (D) Hydroxylation of **1**-H_3 and **1**-D_3[a]

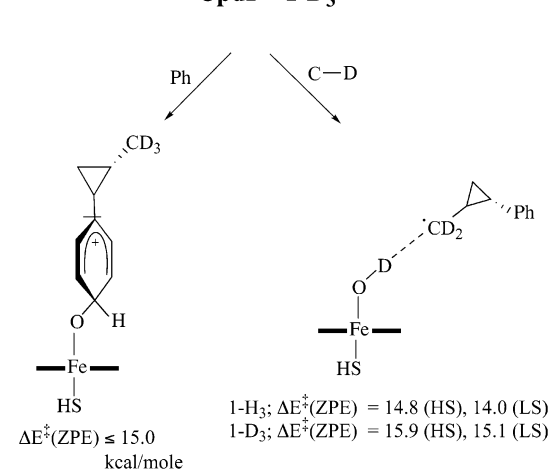

[a] The barriers are corrected by ZPE.

Scheme 7 summarizes the ZPE corrected barriers for the two processes nascent from Cpd I. As we have shown recently,[34] benzene hydroxylation occurs predominantly via a LS cationic mechanism with an intermediate having a major cationic σ-complex character, as indicated in the scheme. The barrier for this process was found to be sensitive to polarity and hydrogen bonding effects and could be estimated as 16.5 kcal/mol for benzene as a substrate. We expect the same LS cationic mechanism to operate during phenyl hydroxylation of probe **1**. But, since the resulting cationic σ-complex species of **1** is expected to be significantly more stable than the corresponding species for benzene, a concomitant reduction of the barrier can be safely assumed for the phenyl hydroxylation in **1**. Considering the cyclopropyl effect on cationic centers (e.g., from solvolytic reactions), this reduction would be at least 1.5 kcal/mol; i.e., the phenyl hydroxylation barrier in **1** will be reduced down to ≤15 kcal/mol, as indicated in Scheme 7. At the same time, the complete isotopic substitution increases the barriers for C−H hydroxylation of **1**, by more than 1 kcal/mol, and the barriers become >15 kcal/mol (Scheme 7). Clearly, based on the computational data for Cpd I alone, we can deduce that the LS hydroxylation of the phenyl group and the two-state hydroxylation of the CD_3 group will be competitive for a probe like **1**.

This fine balance can be further appreciated by the use of substituents that affect more the cationic mechanism of phenyl hydroxylation and can therefore either accelerate phenyl hydroxylation or depress it, while hardly affecting C−H hydroxylation. For example, electron-withdrawing substituents on the phenyl group of **1** would destabilize the putative cation (like **1**-σ(Ph^+) in Scheme 7) relative to that in benzene, thereby causing the barrier for phenyl hydroxylation to exceed 16.5 kcal/mol. Phenyl hydroxylation will then cease to be competitive with C−H hydroxylation. Experimental data with the p-CF_3 substituted substrate[45,50] indeed only shows C−H hydroxylation. An interesting speculation, which would require a proof, by QM/

(49) See pages 129−134 in ref 43.
(50) Toy, P. H.; Coon, M. J.; Vaz, A. D. N. *J. Am. Chem. Soc.* **1998**, *120*, 9718−9719.

Scheme 8. Resonance Structures Which Contribute to the Electronic Structures of "$^2\mathbf{I}_U(\mathbf{1})^+$" and $^2\mathbf{I}_U(\mathbf{4})^+$; (a) Is the Major Contributor to "$^2\mathbf{I}_U(\mathbf{1})^+$", while (b) Is the Major Contributor to $^2\mathbf{I}_U(\mathbf{4})^+$

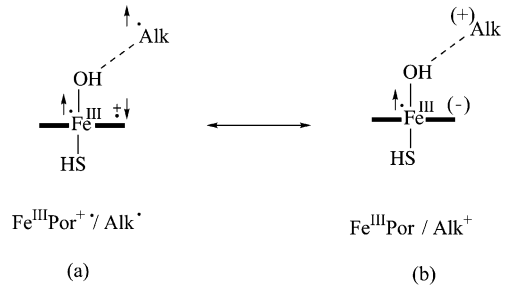

MM calculations, is that the observed effect of the mutation (Thr → Ala) in the distal pocket of P450[45,50] which increases the relative Ph/CH_3 oxidation ratio for **1** is due to changes in the topography/polarity of the pocket that favor the LS cationic mechanism of phenyl hydroxylation over the radical TSR mechanisms of C−H hydroxylation. *This reactivity interplay of the different state situations may masquerade as two different oxidants*.[24]

4.D. On the Status of Carbocation Intermediates in the C−H Hydroxylation of 1 and 4. As mentioned in the Introduction, some predesigned probes, such as the one in Scheme 2, were found to rearrange in a pattern that indicates the presence of carbocationic intermediates.[15] Small amounts of cationic-derived products were also observed in other probes.[6b] This in turn raises the question on substrates such as **1** and **4**, where radicals and carbocations would be expected to rearrange alike, thus casting doubts on the identity of the species undergoing rearrangement.[15−18]

Our results, in Figure 1 vs 10, show that, in the case of **1**, the rearranging species are definitely the carbinyl radicals complexed to iron−hydroxo (shown as $^{2,4}\mathbf{I}_U$ in Figure 3). As described in the results section, an attempt to generate a cationic intermediate by shifting the electron from the carbinyl moiety to the heme resulted in the "$^2\mathbf{I}_U{}^+(\mathbf{1})$" species in Figure 10. Even with the inclusion of medium polarity effects, the charge on the alkyl moiety reached only +0.27. This and the large spin density on both the alkyl as well as on the porphyrin moieties show that the "$^2\mathbf{I}_U{}^+(\mathbf{1})$" species are more akin to an LS state $HS^-Fe(III)Por^{+\bullet}OH/Alk^{\bullet}$ species. However, the fact that the total spin density computed for "$^2\mathbf{I}_U{}^+(\mathbf{1})$" does not sum up to three electrons indicates that it is a mixed valent species of the type shown in Scheme 8.[51] Thus, the "$^2\mathbf{I}_U{}^+(\mathbf{1})$" species has a major $HS^-Fe(III)Por^{+\bullet}OH/Alk^{\bullet}$ character in resonance with a minor $HSFe(III)PorOH^-/Alk^+$ contribution. In brief, the calculations show that the question of cationic rearrangement products does not pertain to the probe substrate **1**.

As can be seen in Figure 10, the "$^2\mathbf{I}_U{}^+(\mathbf{4})$" species exhibits a more pronounced carbocationic character, which is understandable since the radical center is substituted by two methyl groups that stabilize a positive charge. Nevertheless, the fact that the alkyl charge is only +0.6 indicates an intimate ion pair

(51) A natural orbital analysis indicates that the species behaves as a mixed-valent state where the electron resides partly on the radical and partly on the porphyrin in the a_{2u} orbital. This feature is from the orbitals that contain the population of 1.5 and $0.5e^-$ and corresponds to the bonding and antibonding combinations of the radical orbital, ϕ_c, and the a_{2u} orbital (the mixing is mediated by the π^* orbitals of the FeO moiety). As such, this species is a highly conjugated intimate ion pair, with a preponderant radical character.

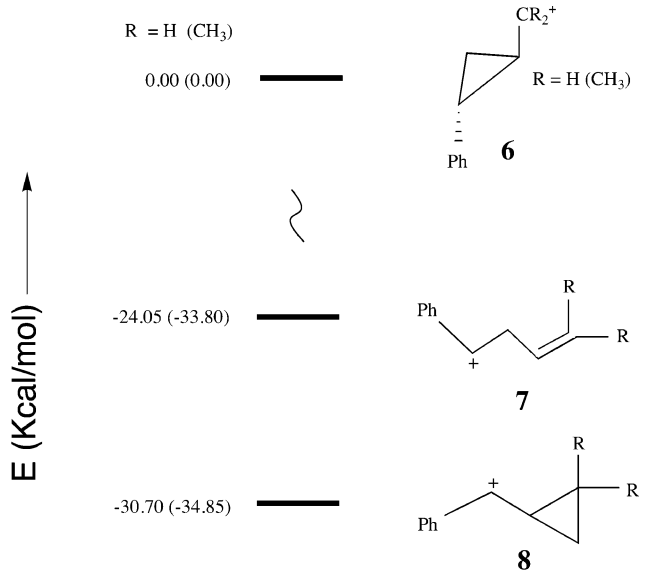

Figure 11. 6-31G* relative energies (kcal/mol) of the isomers of the carbocations derived from probe substrates **1** (R = H) and **4** (R = CH_3). In fact, the only stable species are **7** and **8**, while cation **6** is optimized under constraints.

of the type shown in Scheme 8, where now the HSFe(III)-$PorOH^-/Alk^+$ form is dominant though not the exclusive one. Since the intimate ion pair enjoys O- - -C bonding as well as electrostatic stabilization from the negative heme moiety in the major form (see part b, Scheme 8), a "free" cationic intermediate is excluded in our calculations. Furthermore, having this intimate ion pair character, with partial C- - -O bonding, drives the species toward rebound without rearrangement. Indeed, as discussed in the Results section "$^2\mathbf{I}_U{}^+(\mathbf{4})$" is not a true intermediate but rather a species on the downhill rebound pathway en route to the unrearranged ferric-alcohol product (**5** in Figure 7).

Despite the above analysis, we cannot rule out the possibility that in cases such as $^2\mathbf{I}_U{}^+(\mathbf{4})$ or even "$^2\mathbf{I}_U{}^+(\mathbf{1})$" the electric field and hydrogen bonding machinery of the protein environment may stabilize true ion pair $HSFe(III)PorOH^-/Alk^+$ intermediates and may even give rise to small amounts of free (diffusive) carbocations, as proposed in the recent study of Ortiz de Montellano, Groves et al.[6b] To test this possibility for **1** and **4**, one must first elucidate the types of rearrangement expected from such free carbocations, which are displayed in Figure 11. As shown in the figure, the unrearranged Alk^+ moiety, **6**, lies considerably higher than the rearranged isomer **7** with the benzylic cationic center. But the most stable form is **8**, in which the cationic center is stabilized by both the phenyl and the cyclopropyl groups. Clearly, were free carbocations present during C−H hydroxylation of these substrates, one would have expected to find at least some hydroxylation products derived from **8**. Since such products, to the best of our knowledge, have never been observed, this fact further weakens the case for the involvement of carbocations during hydroxylation of **1** and **4**. Clearly, therefore, the significant amount of rearranged product, **3** (Figures 1 and 3), that has been observed[15] in the C−H hydroxylation of **1** must have arisen from the HS radical complex intermediate, $^4\mathbf{I}_U$ (Figure 1), whereas no rearrangement and no signs of carbocations were detected for **4**.[15]

5. Conclusions

The above study addresses the major controversies, which surround the 'rebound mechanism',[2,6] and which have emerged from a decade of mechanistic studies of probe substrates[15,30] that generate radical clocks upon initial hydrogen abstraction. These studies have revealed lifetimes of radicals that are too short, rearranged products which indicate that carbocations are involved rather than radicals,[15] and a distinct product isotope effect which rule out the possibility that the various products are generated from a single pathway, with a single intermediate that branches into two products.[30] The present paper is the first extensive theoretical treatment that addresses the heart of these controversies by elucidating the C−H hydroxylation mechanisms of two Newcomb probe substrates,[15,30] *trans*-2-phenyl-methyl-cyclopropane (**1**) and *trans*-2-phenyl-*iso*-propylcyclopropane (**4**). The theoretical study of these experimental systems reveals that the only low energy pathway for C−H hydroxylation is *the two-state rebound mechanism* with high-spin (HS) and low-spin (LS) manifolds, as described originally for methane hydroxylation.[25] The key theoretical results and conclusions are the following:

(a) Two-state reactivity (TSR) leads to a good match to experimental results concerning the very different extents of rearrangement for **1** (20−30%) vs **4** (virtually none). Furthermore, it is shown that these computational trends can be (and were[44]) predicted directly from simple reasoning of the factors that determine the height of the rebound barrier on the HS manifold.[25,27,44]

(b) Use of TSR to calculate intrinsic product isotope effect ($PIE(\mathbf{2}/\mathbf{3})_{TSR}$) for the unrearranged (**2**) and rearranged (**3**) products of substrate **1** leads to values in the same direction as the experimental result determined from the study of intramolecular isotope effect.[30] The fit of the $PIE(\mathbf{2}/\mathbf{3})_{TSR}$ and $PIE(\mathbf{2}/\mathbf{3})_{obs}$ quantities for intermolecular isotope effect is ambiguous.[30,47] The observed quantity may reflect masking of the intrinsic value (see eq 5) and its influence by other branching processes, e.g. phenyl hydroxylation which occurs mainly from the LS manifold.

(c) Comparison of the calculated barriers for C−H hydroxylation in **1** and those calculated before for phenyl hydroxylation[34] enables us to predict the experimentally observed[47,50] regioselectivity reversal (metabolic switching) from C−H to phenyl hydroxylation, when the methyl group of **1** is fully deuterated. It also enables us to rule out such a reversal for the *p*-CF_3 substituted probe, again in accord with experiment.

(d) The study shows that carbocations that appear as intimate ion pair species, $HSFe(III)PorOH^-/Alk^+$, in the case of **4** give no rearranged products. The lack of rearrangement for **4** is in accord with experimental data.[15] Generally, for other substrates a small amount of carbocations (as observed, e.g., in ref 6b) can be generated by minor dissociation of intimate ion pairs or by electron transfer[6b] from the corresponding radical complexes, $HSFe(IV)PorOH/Alk^{\bullet}$. The rearrangement patterns of the carbocations derived from **1** and **4** were analyzed. On the basis of the expected products, it was possible to exclude carbocations in the cases of **1** and **4**.

All in all, the study shows that the TSR scenario of a two-state rebound mechanism by Cpd I accommodates much of the experimental data and resolves the major controversies in a coherent manner; the match approaches a proof that TSR is the actual mechanism in experimental systems. In this sense, the study reveals that the *intrinsic product isotope effect* is a sensitive experimental probe of TSR, with a clear physical significance; *the size of the intrinsic product isotope effect and its direction reveal the structural differences of the hydrogen abstraction transition states in the LS vs HS reaction manifolds*. The observed product isotope effect may involve, however, other effects, which may mask the intrinsic quantity.

Finally, the rebound processes of the rearranged radicals, in Figures 5 and 6, reveal for the first time a significant barrier for the LS rebound process due to the loss of resonance energy of the rebounding radicals. It has not escaped the attention of the authors that these results may have bearing on the understanding of the asymmetric hydroxylation of ethylbenzene and similar substrates[2,52,53] and its possible interpretation.[6b]

Acknowledgment. *The paper is dedicated to K. N. Houk on the occasion of his 60th birthday*. The research was supported by a grant to S.S. by the Israel Science Foundation (ISF).

Note Added in Proof. A recent paper (Chandrasena, R. E. P.; Vatsis, K. P.; Coon, M. J.; Hollenberg, P. F.; Newcomb, M. *J. Am. Chem. Soc.* **2004**, *126*, 115−126) reveals that PIE for **1**-*p*CF_3 is >1 and that the intermolecular KIEs are masked. For **1** the intermolecular values lead to PIEs in the range 1.4−2.3.

Supporting Information Available: Tables (23) and figures (22) with computational data. This material is available free of charge via the Internet at http://pubs.acs.org.

JA039439S

(52) Groves, J. T.; Visky, P. *J. Org. Chem.* **1990**, *55*, 1269−1272.
(53) Groves, J. T.; Visky, P. *J. Am. Chem. Soc.* **1989**, *111*, 8537−8538.